ACS APPLIED NANO MATERIALS

www.acsanm.org Letter

Polyniobate Nanothreads for Decomposition of the Nerve Agent Simulant Dimethyl Chlorophosphate

Yiyao Tian, Alexey L. Kaledin, Daniel L. Collins-Wildman, Victoria G. Snider, Djamaladdin G. Musaev,* Craig L. Hill,* and Anatoly I. Frenkel*

Cite This: *ACS Appl. Nano Mater.* 2021, 4, 5649–5654 Read Online

ACCESS | Metrics & More | Article Recommendations | Supporting Information

ABSTRACT: The nanoscale one-dimensional polymeric polyniobate $K_{12}[Ti_2O_2][SiNb_{12}O_{40}]\cdot 22H_2O$ (**KSiNb**) rapidly hydrolyzes the gaseous organophosphorus nerve agent simulant dimethyl chlorophosphate (DMCP). A multimodal approach combining X-ray, IR and Raman spectroscopies and computation reveals that this reaction, involving the initial nucleophilic attack of polyoxometalate (POM) oxygen at phosphorus, is greatly modulated by the polyniobate counterions: the most negative and nucleophilic oxygen atoms in **KSiNb**, the Ti−O−Ti and Ti−O−Nb oxygen atoms, preferentially bind the potassium counterions, compelling the less negative oxygen atoms to become the nucleophiles. This heretofore unnoted paradigm of the POM counterion location and function could well impact a myriad of POM reaction studies.

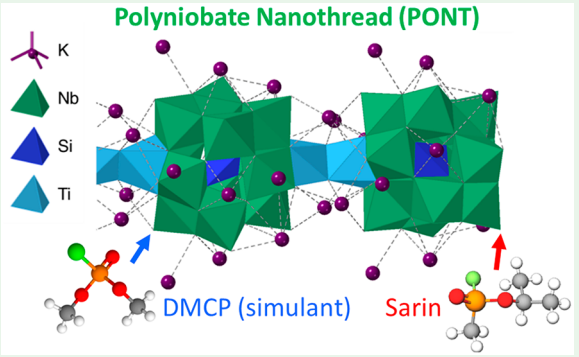

KEYWORDS: *polyniobates, counterion impacts, nerve agent, X-ray absorption spectroscopy, DRIFTS, density functional theory, normal-mode analysis*

1. INTRODUCTION

Strategies for chemical warfare agent (CWA) decontamination to protect both military and civilian populations from their significant threat have been investigated for decades.[1,2] In particular, organophosphorus (OP) nerve agents, one class of CWAs, are generally detoxified via hydrolysis. Several types of materials for hydrolysis of OP nerve agents and simulants have been proposed,[3,4] notably metal−organic frameworks (MOFs) and polyoxometalates (POMs).

MOFs are a class of hybrid organic−inorganic coordination polymers formed by inorganic cores connected by organic linkers to form extended networks with high porosity and ultrahigh surface areas.[5] A series of Zr-based MOFs, especially UiO-66, UiO-67, NU-1000, and MOF-808, which contain acidic Zr^{IV} sites, have been proven to hydrolyze nerve agents and the simulants dimethyl 4-nitrophenylphosphate (DMNP)[6,7] and dimethyl methylphosphonate (DMMP).[8,9] Importantly, open-pore structures and the presence of defects are key requirements in Zr_6-based MOFs to enable OP nerve agent hydrolysis. However, the vapor-phase exposure of organophosphonates to these MOFs leads to the strongly bound products at the Zr_6-based MOF nodes or to the MOF collapse. Both of these effects lead to the diminution or loss of catalytic reactivity. Inhibition of catalytic hydrolysis activity has been extensively reported in solution[6] and more recently reported to render these MOFs ineffective as catalysts for gas-phase CWA hydrolysis.[8,9]

POMs comprise a group of molecular, highly tunable, metal−oxygen anions with versatile applications in magnetism, medicine, electrochemistry, and catalysis[10,11] that have also been investigated for the decontamination of CWAs and/or their simulants.[12−16] Multiple classes of POMs have been shown to catalyze hydrolysis of OP nerve agents, including polymolybdates, polyniobates, and polytungstates.[17−22] Nyman and co-workers reported a one-dimensional polymeric polyniobate, $K_{12}[Ti_2O_2][SiNb_{12}O_{40}]\cdot 22H_2O$ (**KSiNb**),[23,24] whose structure is given in Figure 1, and its isostructural analogue **KGeNb**. **KSiNb** can be referred to as polyoxoniobate nanothreads (PONTs) based on the reported X-ray crystallography. The cross section of **KSiNb** is ∼1.5 × 1.5 nm, while along the arbitrarily long chain, the Keggin POM unit is ∼1.5 nm × 1.5 nm × 1.4 nm.[23] The Keggin chains crystallize together, forming the particles seen in the scanning electron microscopy (SEM) images described in greater detail below. The components of PONTs, like those of MOFs, can be modified extensively, and PONTs can be easily prepared in large quantities.

Received: March 23, 2021
Accepted: June 1, 2021
Published: June 7, 2021

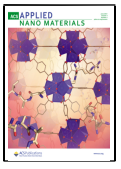

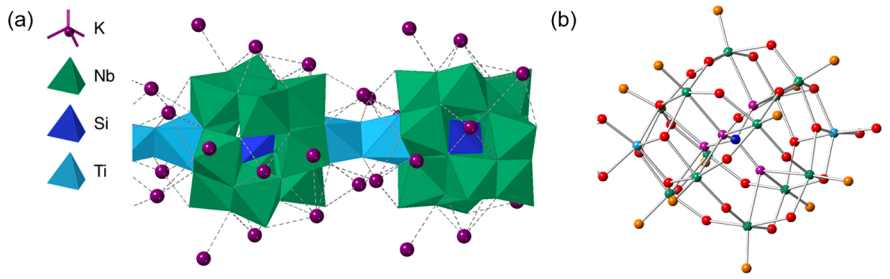

Figure 1. (a) Schematic of the **KSiNb** structure including the potassium counterions. The dashed lines shown for the K−O bonds are present where any K−O bond is less than 3.5 Å. Reproduced from ref 21. Copyright 2016 Wiley-VCH. (b) Fragment of the ball−stick **KSiNb** structure that shows terminal (O^t, orange), bridging (O^b, red), and central (O^c, purple) O atoms in polyniobates.

Subsequent to the report of these PONTs, we reported that they are more reactive than hydroxide for hydrolysis of Sarin (GB) and its simulants in either solution or the gas phase.[21] However, no details are known about this **KSiNb**-catalyzed hydrolysis of OP compounds. The following key questions remain unanswered: (a) What are the active site atom(s) of **KSiNb** that facilitate docking of the OP compound? (b) Which of these atoms attack the OP compound? (c) What are the roles of the many countercations of **KSiNb** in this hydrolytic chemistry (structure in Figure 1)? (d) What factors might destabilize **KSiNb** in the course of catalytic turnover? This paper addresses these questions using **KSiNb** and the GB simulant dimethyl chlorophosphate (DMCP).

A combination of methods is the key for studying the activity mechanisms of nanoscale filtration materials.[6] In this work, diffuse-reflectance infrared Fourier transform spectroscopy (DRIFTS), an X-ray absorption fine structure (XAFS) study of the key components in the PONT (**KSiNb** in the present case) architecture, Raman spectroscopy, density functional theory (DFT) calculations, and normal-mode analysis were combined for illuminating the details of the DMCP and PONT interaction and the DMCP decomposition by the PONT. In the course of this investigation, a key issue emerged, namely, that the PONT countercations charge-neutralize and sterically block the most negative O atoms[25,26] by strong association with these O atoms. While the roles of POM counterions on the self-assembly, stabilization, and solubility of POMs were recently reviewed[27] and detailed quantitative studies on the roles of alkali-metal counterions on POM redox reactivity have also been reported,[28,29] this study through the use of all of the experimental and computational approaches noted above reveals for the first time a selective, preferential steric blocking and neutralization of the most negative POM O atoms that shifts the reactivity to conventionally less negative and reactive O atoms. The combined study revealed the location of reaction-active O sites in the **KSiNb** structure.

2. RESULTS AND DISCUSSION

KSiNb was synthesized according to reported literature methods; the purity was confirmed via Fourier transform infrared (FTIR; Figure S1).[24] The morphology of **KSiNb** particles can be seen in the SEM image (Figure S2). **KSiNb** nanothreads crystallize together to form rodlike particles consisting of many polyniobate chains. Energy-dispersive X-ray analysis (EDX) confirms the uniform nature of the material (Figure S3).

All of the experimental and computational studies on **KSiNb** presented here include all of the countercations of this polymeric polyanion. To probe the adsorption of DMCP on **KSiNb** at the gas−solid interface, we performed DRIFTS experiments (Figure 2). Assignment of the bands that emerge

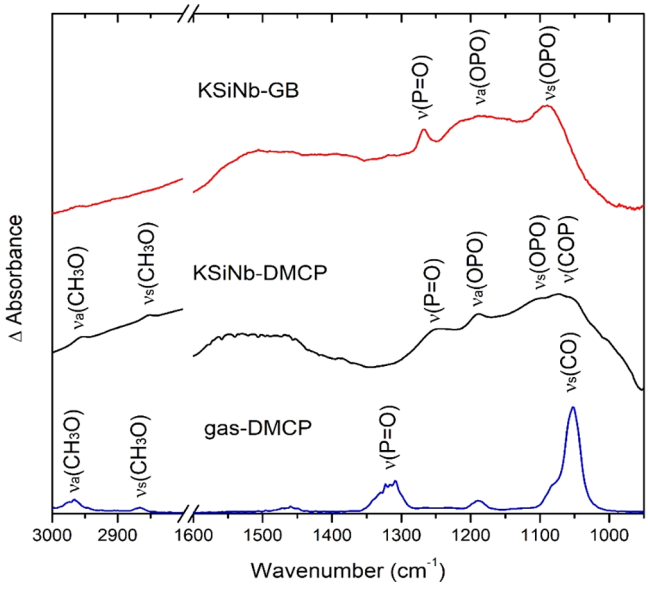

Figure 2. Difference DRIFTS spectra of (top) GB adsorption and hydrolysis on **KSiNb**, (middle) DMCP adsorption and hydrolysis on **KSiNb**, and (bottom) gas-phase DMCP. The top and bottom curves are from ref 30. Copyright 2012 American Chemical Society.

upon exposure is aided by a direct comparison of the spectra of gas-phase DMCP.[30] The peak observed at 1255 cm^{-1} was assigned to the ν(P═O) stretch of chemisorbed DMCP on the **KSiNb** sample. This peak redshifts from the gas-phase DMCP value for this mode of 1309 cm^{-1}, which is also observed in the calculated IR spectra of chemisorbed DMCP on **KSiNb**, where this mode redshifts by about 50 cm^{-1} from the gas-phase DMCP as well (Figure S4). The peak observed at 1188 cm^{-1} and the overlapping bands between 1130 and 1040 cm^{-1} are assigned to ν_a(O−P−O), ν_s(O−P−O), and ν(C−O−P) stretches, mixed in with modes belonging to DMCP-derived products.[8,9] These bands, together with the appearance of phosphate species with exposure, confirm the adsorption and decomposition of DMCP on **KSiNb**. Upon DMCP exposure, the decrease of the broad peak intensity at ∼3400 cm^{-1} observed in the ν(O−H) stretching region in pristine **KSiNb** suggests the loss of bonded water (Figure S5), as supported by a decrease in the band intensity during thermal treatment. The perturbation of water molecules suggests the hydrolysis of DMCP by **KSiNb**, which is consistent with the

https://doi.org/10.1021/acsanm.1c00813
ACS Appl. Nano Mater. 2021, 4, 5649−5654

mechanism proposed for the hydrolysis of DMMP by $K_{12}[Ti_2O_2][GeNb_{12}O_{40}]\cdot 19H_2O$ (**KGeNb**) and **KSiNb**.[21] In order to evaluate the quality of DMCP as a simulant for GB, a direct comparison of the spectra of DMCP- and GB-treated **KSiNb** is shown in Figure 2. Similar effects were observed when **KSiNb** was exposed to GB, namely, the appearance of ν(P═O) and ν(O−P−O) stretches, suggesting a strong similarity in the surface chemistry of DMCP and GB. Therefore, DMCP is a reasonable simulant for GB deactivation studies in battlefield-relevant conditions.

To investigate the active sites in the reaction of **KSiNb** with DMCP and to understand the reaction mechanism, characterization techniques that are sensitive to changes of the local environment of **KSiNb**, and, especially, metal−oxygen bonds, before and after DMCP exposure are needed. For this purpose, we conducted XAFS and Raman spectroscopy experiments. XAFS experiments were performed at National Synchrotron Light Source II (NSLS-II) at BNL. Ti K-edge and Nb K-edge measurements were conducted on beamlines 8-ID (ISS) and 7-BM (QAS), respectively. The behavior of the Ti K-edge X-ray absorption near-edge structure (XANES) spectra of **KSiNb** before and after DMCP exposure (Figure S6) suggests that the interaction of **KSiNb** with DMCP keeps the TiO_6 linkage intact, indicating the stability of the molecular and polymeric structures. The Fourier transform magnitude of the Nb K-edge extended X-ray absorption fine structure (EXAFS) spectra in **KSiNb** decreases upon DMCP exposure, suggesting an increase in disordering of the Nb−O bonds and/or a decrease in the Nb coordination number.

To understand the detailed structural changes of the Nb environment, quantitative EXAFS analysis was performed. Because of the complexity of the **KSiNb** structure (Figure 1), the histogram of Nb bond types and a bond length distribution from 1.5 to 4.0 Å was calculated from the known crystal structure[12,21] and is plotted in Figure S7. As the histogram shows, the nearest-neighbor coordination shells of Nb−O cannot be described by one effective shell. Instead, we divided them into three effective shells [Nb−O1, Nb−O2, and Nb−O3, representing terminal (O^t), bridging (O^b), and central (O^c) O atoms in polyniobates] and assigned to each of them the coordination number calculated from the bond distribution histogram (Figure S7 and Table S1). Nb K-edge EXAFS data and theoretical fits are shown in Figure S8. The best-fit results for the structural parameters are shown in Table 1 and Table S1. All of the defined Nb−O bonds were used for calculating the fluctuations. Therefore, the averaged quantities reported in Table 1 include contributions from the entire complex (Tables S2−S4). The results for pristine **KSiNb** are consistent with the information available from the crystal structure data.[23] The main finding from quantitative EXAFS analysis is that the shortest bonds between the Nb and O atoms (labeled O^t in Figure 1 and Table 1) respond to the strongest during the interaction with DMCP by a significant increase in bond-length disorder. Compared to the Nb−O^t pairs, the mean-squared disorder in the Nb−O distances for the Nb−O^b pairs vary by much smaller relative amounts (Table 1) after DMCP exposure. The observed strong response to DMCP in the Nb−O^c distance fluctuations is a second-order effect arising from a strong correlation with the conjugate Nb−O^t bond interacting with DMCP.

In summary, the XAFS results demonstrate the stability of the polymeric structure in **KSiNb** and that the O_t atoms of polyniobates are most responsive when interacting with

Table 1. Mean-Squared Bond-Length Disorder Values, σ^2 (Å^2), Obtained from the Fits of the Experimental EXAFS Data (Uncertainties in the Last Significant Digits Are Shown in Parentheses) and Calculated for KSiNb in a Framework of a Quantum Harmonic Oscillator Model at 298 K, Using the Normal Modes at the Corresponding Global Minima at the wB97XD/6-31G(d,p)+LANL2DZ Level of Theory[a]

system	experiment/ theory	Nb−O^t	Nb−O^b	Nb−O^c
KSiNb (pristine)	experiment	0.0047(10)	0.0102(7)	0.0102(7)
KSiNb-DMCP	experiment	0.0096(20)	0.0148(10)	0.0148(10)
KSiNb (pristine)	theory	0.0016	0.0097	0.0103
KSiNb−DMCP physisorbed	theory	0.0016	0.0097	0.0102
KSiNb−DMCP chemisorbed	theory	0.0067	0.099	0.0167

[a]The disorder values were calculated for Nb−O pairs corresponding to the terminal (O^t), bridging (O^b), and central (O^c) atoms.

DMCP. In addition, the feature assigned to Nb−O^t in Raman spectra[19] of DMCP-exposed **KSiNb** (Figure 3b) blueshifts from this mode in pristine **KSiNb**, which is also observed in the calculated Raman spectra of chemisorbed DMCP on **KSiNb** (Figure 3c). These findings support the XAFS results and lead us to hypothesize that Nb−O^t are active sites for DMCP decomposition.

In order to explain these findings, we conducted corresponding simulations to uncover the details of the reaction mechanism and the nature of the structural response within **KSiNb** during reactions with DMCP. The specific questions of interest are as follows: Can we distinguish between the effects of physisorbed DMCP and the decomposition products on **KSiNb**? What are the static (configurational) and dynamic contributions to the experimentally measured bond-length disorder, and what are their relative changes upon DMCP adsorption and decomposition? Finally, what roles do the countercations have on these phenomena and the structures and reactivity of **KSiNb** and related POMs in general?

Following an exhaustive structural analysis, the DFT calculations revealed two types of **KSiNb**−DMCP interactions, a weaker bound physisorbed complex, labeled **KSiNb**−$DMCP_p$ (Figure 4, top), and a much stronger bound chemisorbed complex, labeled **KSiNb**−$DMCP_c$ (Figure 4, bottom). The **KSiNb**−DMCP electronic and free energy (at 298 K) interactions for **KSiNb**−$DMCP_p$ are $\Delta E = -18.5$ kcal/mol and $\Delta G = -5.7$ kcal/mol, respectively, relative to the **KSiNb** + DMCP dissociation limit. In **KSiNb**−$DMCP_p$, we identified four hydrogen bonds involving two O^b and two O^t sites and one O−K^+ interaction (with a 2.9 Å O−K^+ distance). The calculations show that the **KSiNb**−$DMCP_c$ complex formation involves P−Cl bond cleavage, P−O^t bond formation, full rupture of the Nb−O^t bond (from 1.77 Å in pristine **KSiNb** to 2.12 Å in the chemisorbed complex), and a strengthening and decreasing of a Nb−O^c bond (from 2.43 to 2.08 Å). Interestingly, the product Cl^- ion drifts away from P and coordinates with a few available K^+ sites. In other words, the reaction may be loosely characterized as an interaction of O^t in **KSiNb** with a DMP^+ unit that, nonetheless, is mitigated

https://doi.org/10.1021/acsanm.1c00813
ACS Appl. Nano Mater. 2021, 4, 5649−5654

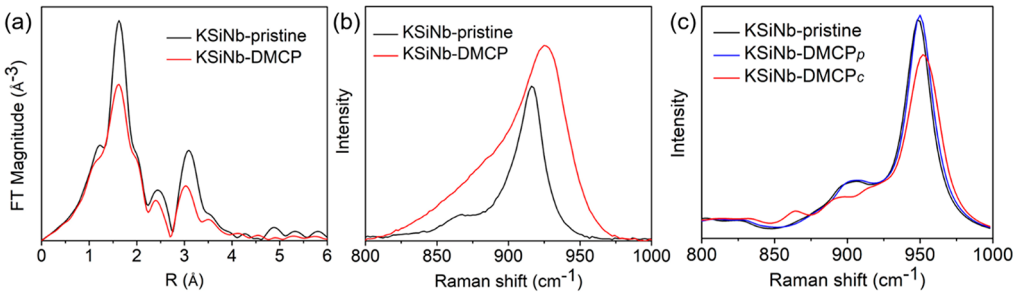

Figure 3. (a) Fourier transform magnitude of k^2-weighted Nb K-edge EXAFS spectra for pristine and DMCP-treated **KSiNb**. (b) Experimental and (c) calculated Raman spectra in the Nb−O^t region. Physisorbed and chemisorbed **KSiNb**−DMCP complexes are indicated by subscripts *p* and *c*, respectively.

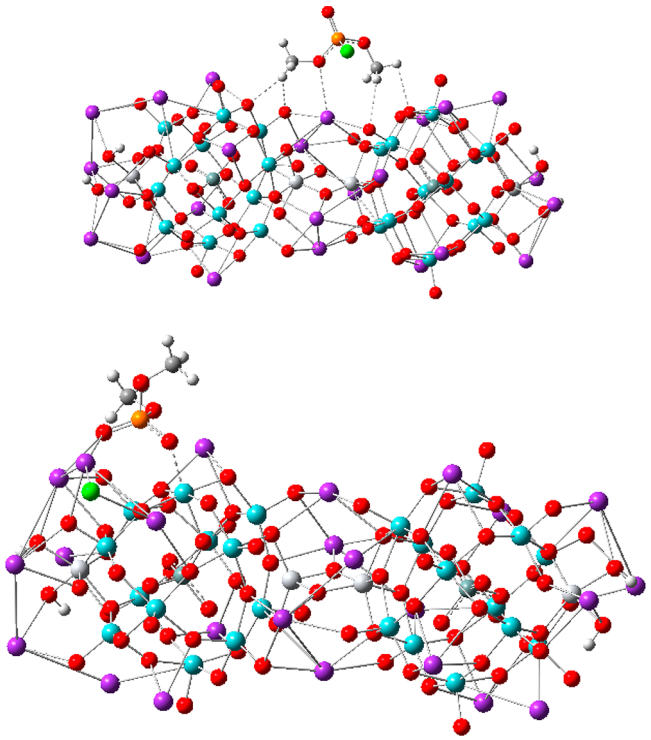

Figure 4. Top: Ball-and-stick representation of simulated physisorbed DMCP on **KSiNb**. The H−O distances marked by dashed bonds are 2.3, 2.4, 2.9, and 2.6 Å, respectively. The O−K distance is 2.9 Å. Color code: K, purple; O, red; Nb, cyan; Si, dark cyan; Ti, light gray; P, orange; Cl, green; C, gray; H, smaller light-gray balls. Bottom: Ball-and-stick representation of simulated chemisorbed DMCP on **KSiNb**. P−O^t = 1.54 Å, Nb−O^t = 2.12 Å, Nb−O^c = 2.08 Å, and Cl−K = 3.1 Å. Color code: K, purple; O, red; Nb, cyan; Si, dark cyan; Ti, light gray; P, orange; Cl, green; C, gray; H, smaller light-gray balls.

to some extent by an incoming H_2O molecule reminiscent of an S_N2 reaction. The calculated electronic and Gibbs free energies of the reaction **KSiNb** + DMCP → **KSiNb**−DMCP$_c$ are −79.7 and −67.2 kcal/mol, respectively. Thus, the formation of **KSiNb**−DMCP$_c$ upon the interaction of **KSiNb** with gaseous DMCP is strongly exergonic.

To estimate the role of the presence of water molecules, the interaction of **KSiNb** with a single water molecule was studied. We found that **KSiNb**−H_2O (Figure S9 and Table S5) was stable relative to the **KSiNb** + H_2O dissociation limit by ΔE/ΔG(298 K) = −18.3/−7.6 kcal/mol. We note that an increase in the temperature to 350 K decreased the thermal stability of **KSiNb**−H_2O to ΔG(350 K) = −6.0 kcal/mol, supporting the argument of a partial loss of water upon thermal treatment, a finding that is fully consistent with the well-established general behavior of hydrated POMs and metal oxide nanoparticles.

The calculations of bond variance (see Table 1 and the Supporting Information for calculation details) reproduce the experimentally observed trends and provide answers on the identified dramatic reduction in the XAFS intensity (Figure 3a) for the DMCP-exposed **KSiNb**. Also DFT calculations of **KSiNb**−DMCP$_c$ qualitatively reproduce the Raman results: As seen in Figure 3b,c, a blue shift of the 950 cm^{-1} peak is clearly visible in the chemisorbed spectrum. This finding enables us to conclude that the Raman data reflects the chemisorbed complex **KSiNb**−DMCP$_c$. Analysis of the vibrational dynamics confirms that the broad peak at 950 cm^{-1} is a cluster of Nb−O^t stretching modes. In the chemisorbed species, the Nb−O^t stretch shifts away to the red by almost 400 cm^{-1}, while inspection of the force constants (FCs) in the 920−970 cm^{-1} range, i.e., that corresponding to the true Nb−O^t stretch, shows that the average FC increases from 0.40 hartree/bohr^2 in **KSiNb** to 0.48 hartree/bohr^2 in **KSiNb**−DMCP$_c$. Thus, the blue shift seen in Figure 3b,c is a direct result of the increased FC of the remaining "free" Nb−O^t bonds. We speculate that this increase in the Nb−O^t FC is due to electron density reorganization following the removal of one, or more O_t atoms by DMCP, depending on the number of interacting nerve agent molecules.

Significantly, the collective data (XAFS data, Raman shifts, and their theoretical modeling results) clearly indicate that the most negatively charged O atoms, those bridging the Ti(IV) centers, are not interacting with DMCP because they are preferentially bound to the more positive K countercations. While the P(V) center of nerve agents and the DMCP simulant are quite electrophilic, they are not as electrophilic as an actual cation, K^+. This neutralization of the O atoms in **KSiNb**, very likely other PONTs and quite possibly all POMs in nucleophilic or general base reactions, by their countercations tracks with the intrinsic basicity of the particular type of O atom. Specifically, the O_b atoms in the Ti(IV)−O−Ti(IV) and Ti(IV)−O−Nb(V) linkages are the most basic, most neutralized, and most sterically blocked from docking and reacting with electrophiles, e.g., DMCP in this study, by their countercations. The next most basic and thus neutralized and sterically blocked by the countercations are the O_b atoms of the Nb(V)−O−Nb(V) linkages. The least cation-neutralized are the O_t atoms, Nb(V)−O^t, and it is these that show the most reactivity in the present multimodal study.

https://doi.org/10.1021/acsanm.1c00813
ACS Appl. Nano Mater. 2021, 4, 5649−5654

3. CONCLUSIONS

Through the use of advanced synchrotron and other spectroscopic techniques, X-ray crystallography, and computational methods, we revealed a specific role of the counterions in the reactivity of metal oxide-like materials (or PONTs) for the hydrolytic decomposition of OP compounds such as CWAs by the O atoms in these structures. We also demonstrated atomic-level details of the binding of a Sarin simulant, DMCP, to a polyoxoniobate material. This study showed that the sites of reactivity are not the most negative and thus traditionally most nucleophilic O atoms but rather the least negative ones because the countercations preferentially associate with, charge neutralize, and sterically block the more reactive ones. This work defines one clear future direction: more effective polyniobates and likely other basic POMs for hydrolysis of nerve agents should be possible by using counterions that are larger and associate less strongly than alkali metals, such as K^+ used in this study, with the most negative polyniobate O atoms. Quaternary ammonium ions are one evident class of such counterions.

■ ASSOCIATED CONTENT

Supporting Information

The Supporting Information is available free of charge at https://pubs.acs.org/doi/10.1021/acsanm.1c00813.

Materials, methods including DRIFTS, XAFS, Raman spectroscopy, and computational methodology, supporting figures and tables, and references (PDF)

■ AUTHOR INFORMATION

Corresponding Authors

Djamaladdin G. Musaev − *Cherry L. Emerson Center for Scientific Computation and Department of Chemistry, Emory University, Atlanta, Georgia 30322, United States;* orcid.org/0000-0003-1160-6131; Email: dmusaev@emory.edu

Craig L. Hill − *Department of Chemistry, Emory University, Atlanta, Georgia 30322, United States;* orcid.org/0000-0002-5506-9588; Email: chill@emory.edu

Anatoly I. Frenkel − *Department of Materials Science and Chemical Engineering, Stony Brook University, Stony Brook, New York 11794, United States; Chemistry Division, Brookhaven National Laboratory (BNL), Upton, New York 11973, United States;* orcid.org/0000-0002-5451-1207; Email: anatoly.frenkel@stonybrook.edu

Authors

Yiyao Tian − *Department of Materials Science and Chemical Engineering, Stony Brook University, Stony Brook, New York 11794, United States;* orcid.org/0000-0002-8148-9375

Alexey L. Kaledin − *Cherry L. Emerson Center for Scientific Computation, Emory University, Atlanta, Georgia 30322, United States;* orcid.org/0000-0003-3112-3989

Daniel L. Collins-Wildman − *Department of Chemistry, Emory University, Atlanta, Georgia 30322, United States;* orcid.org/0000-0002-7354-6595

Victoria G. Snider − *Department of Chemistry, Emory University, Atlanta, Georgia 30322, United States*

Complete contact information is available at: https://pubs.acs.org/10.1021/acsanm.1c00813

Author Contributions

D.L.C.-W. and C.L.H. synthesized the samples and performed activity tests. Y.T. and A.I.F. collected and analyzed the XAFS, DRIFTS and Raman spectroscopy data. A.L.K. and D.G.M. performed theoretical modeling. V.G.S. collected the SEM and elemental EDX data. The manuscript was written through contributions of all authors. All authors have given approval to the final version of the manuscript.

Notes

The authors declare no competing financial interest.

■ ACKNOWLEDGMENTS

This work is supported by the U.S. Army Research Laboratory and U.S. Army Research Office under Grant W911NF-15-2-0107. We thank the Defense Threat Reduction Agency for support under Program CB3587. The work with DMCP at the BNL Chemistry Division was made possible because of the Program Development Grant 21-017 to A.I.F. This research used beamlines 7-BM (QAS) and 8-ID (ISS) of the NSLS-II, a U.S. Department of Energy (DOE) Office of Science User Facility, operated for the DOE Office of Science by BNL under Contract DE-SC0012704. This work was performed in part at the Georgia Tech Institute for Electronics and Nanotechnology, which is supported by the National Science Foundation (Grant ECCS-1542174).

■ REFERENCES

(1) Dixon, M.; Needham, D. M. Biochemical Research on Chemical Warfare Agents. *Nature* **1946**, *158* (4013), 432−438.

(2) Kim, K.; Tsay, O. G.; Atwood, D. A.; Churchill, D. G. Destruction and Detection of Chemical Warfare Agents. *Chem. Rev.* **2011**, *111* (9), 5345−5403.

(3) Grissom, T. G.; Plonka, A. M.; Sharp, C. H.; Ebrahim, A. M.; Tian, Y.; Collins-Wildman, D. L.; Kaledin, A. L.; Siegal, H. J.; Troya, D.; Hill, C. L.; Frenkel, A. I.; Musaev, D. G.; Gordon, W. O.; Karwacki, C. J.; Mitchell, M. B.; Morris, J. R. Metal-Organic Framework- and Polyoxometalate-Based Sorbents for the Uptake and Destruction of Chemical Warfare Agents. *ACS Appl. Mater. Interfaces* **2020**, *12* (13), 14641−14661.

(4) Ebrahim, A. M.; Plonka, A. M.; Tian, Y.; Senanayake, S. D.; Gordon, W. O.; Balboa, A.; Wang, H.; Collins-Wildman, D. L.; Hill, C. L.; Musaev, D. G.; Morris, J. R.; Troya, D.; Frenkel, A. I. Multimodal Characterization of Materials and Decontamination Processes for Chemical Warfare Protection. *ACS Appl. Mater. Interfaces* **2020**, *12* (13), 14721−14738.

(5) Zhou, H.; Long, J. R.; Yaghi, O. M. Introduction to Metal−Organic Frameworks. *Chem. Rev.* **2012**, *112* (2), 673−674.

(6) Moon, S. Y.; Liu, Y.; Hupp, J. T.; Farha, O. K. Instantaneous hydrolysis of nerve-agent simulants with a six-connected zirconium-based metal-organic framework. *Angew. Chem., Int. Ed.* **2015**, *54* (23), 6795−9.

(7) Katz, M. J.; Mondloch, J. E.; Totten, R. K.; Park, J. K.; Nguyen, S. T.; Farha, O. K.; Hupp, J. T. Simple and compelling biomimetic metal-organic framework catalyst for the degradation of nerve agent simulants. *Angew. Chem., Int. Ed.* **2014**, *53* (2), 497−501.

(8) Wang, G.; Sharp, C.; Plonka, A. M.; Wang, Q.; Frenkel, A. I.; Guo, W.; Hill, C.; Smith, C.; Kollar, J.; Troya, D.; Morris, J. R. Mechanism and Kinetics for Reaction of the Chemical Warfare Agent Simulant, DMMP(g), with Zirconium(IV) MOFs: An Ultrahigh-Vacuum and DFT Study. *J. Phys. Chem. C* **2017**, *121* (21), 11261−11272.

(9) Plonka, A. M.; Wang, Q.; Gordon, W. O.; Balboa, A.; Troya, D.; Guo, W.; Sharp, C. H.; Senanayake, S. D.; Morris, J. R.; Hill, C. L.; Frenkel, A. I. In Situ Probes of Capture and Decomposition of Chemical Warfare Agent Simulants by Zr-Based Metal Organic Frameworks. *J. Am. Chem. Soc.* **2017**, *139* (2), 599−602.

(10) Miras, H. N.; Yan, J.; Long, D.-L.; Cronin, L. Engineering polyoxometalates with emergent properties. *Chem. Soc. Rev.* **2012**, *41* (22), 7403−7430.
(11) Lv, H.; Geletii, Y. V.; Zhao, C.; Vickers, J. W.; Zhu, G.; Luo, Z.; Song, J.; Lian, T.; Musaev, D. G.; Hill, C. L. Polyoxometalate water oxidation catalysts and the production of green fuel. *Chem. Soc. Rev.* **2012**, *41* (22), 7572−7589.
(12) Kinnan, M. K.; Creasy, W. R.; Fullmer, L. B.; Schreuder-Gibson, H. L.; Nyman, M. Nerve Agent Degradation with Polyoxoniobates. *Eur. J. Inorg. Chem.* **2014**, *2014* (14), 2361−2367.
(13) Ma, F.-J.; Liu, S.-X.; Sun, C.-Y.; Liang, D.-D.; Ren, G.-J.; Wei, F.; Chen, Y.-G.; Su, Z.-M. A Sodalite-Type Porous Metal−Organic Framework with Polyoxometalate Templates: Adsorption and Decomposition of Dimethyl Methylphosphonate. *J. Am. Chem. Soc.* **2011**, *133* (12), 4178−4181.
(14) Mizrahi, D. M.; Saphier, S.; Columbus, I. Efficient heterogeneous and environmentally friendly degradation of nerve agents on a tungsten-based POM. *J. Hazard. Mater.* **2010**, *179* (1), 495−499.
(15) Okun, N. M.; Tarr, J. C.; Hilleshiem, D. A.; Zhang, L.; Hardcastle, K. I.; Hill, C. L. Highly reactive catalysts for aerobic thioether oxidation: The Fe-substituted polyoxometalate/hydrogen dinitrate system. *J. Mol. Catal. A: Chem.* **2006**, *246* (1), 11−17.
(16) Okun, N. M.; Anderson, T. M.; Hill, C. L. Polyoxometalates on cationic silica: Highly selective and efficient O_2/air-based oxidation of 2-chloroethyl ethyl sulfide at ambient temperature. *J. Mol. Catal. A: Chem.* **2003**, *197* (1), 283−290.
(17) Dong, J.; Lv, H.; Sun, X.; Wang, Y.; Ni, Y.; Zou, B.; Zhang, N.; Yin, A.; Chi, Y.; Hu, C. A Versatile Self-Detoxifying Material Based on Immobilized Polyoxoniobate for Decontamination of Chemical Warfare Agent Simulants. *Chem. - Eur. J.* **2018**, *24* (72), 19208−19215.
(18) Li, X.; Dong, J.; Liu, H.; Sun, X.; Chi, Y.; Hu, C. Recoverable amphiphilic polyoxoniobates catalyzing oxidative and hydrolytic decontamination of chemical warfare agent simulants in emulsion. *J. Hazard. Mater.* **2018**, *344*, 994−999.
(19) Wang, Q.; Chapleski, R. C., Jr.; Plonka, A. M.; Gordon, W. O.; Guo, W.; Nguyen-Phan, T. D.; Sharp, C. H.; Marinkovic, N. S.; Senanayake, S. D.; Morris, J. R.; Hill, C. L.; Troya, D.; Frenkel, A. I. Atomic-Level Structural Dynamics of Polyoxoniobates during DMMP Decomposition. *Sci. Rep.* **2017**, *7* (1), 773.
(20) Dong, J.; Hu, J.; Chi, Y.; Lin, Z.; Zou, B.; Yang, S.; Hill, C. L.; Hu, C. A Polyoxoniobate−Polyoxovanadate Double-Anion Catalyst for Simultaneous Oxidative and Hydrolytic Decontamination of Chemical Warfare Agent Simulants. *Angew. Chem., Int. Ed.* **2017**, *56* (16), 4473−4477.
(21) Guo, W.; Lv, H.; Sullivan, K. P.; Gordon, W. O.; Balboa, A.; Wagner, G. W.; Musaev, D. G.; Bacsa, J.; Hill, C. L. Broad-Spectrum Liquid- and Gas-Phase Decontamination of Chemical Warfare Agents by One-Dimensional Heteropolyniobates. *Angew. Chem., Int. Ed.* **2016**, *55* (26), 7403−7.
(22) Tian, Y.; Plonka, A. M.; Ebrahim, A. M.; Palomino, R. M.; Senanayake, S. D.; Balboa, A.; Gordon, W. O.; Troya, D.; Musaev, D. G.; Morris, J. R.; Mitchell, M. B.; Collins-Wildman, D. L.; Hill, C. L.; Frenkel, A. I. Correlated Multimodal Approach Reveals Key Details of Nerve-Agent Decomposition by Single-Site Zr-Based Polyoxometalates. *J. Phys. Chem. Lett.* **2019**, *10* (9), 2295−2299.
(23) Bonhomme, F.; Larentzos, J. P.; Alam, T. M.; Maginn, E. J.; Nyman, M. Synthesis, Structural Characterization, and Molecular Modeling of Dodecaniobate Keggin Chain Materials. *Inorg. Chem.* **2005**, *44* (6), 1774−1785.
(24) Nyman, M.; Bonhomme, F.; Alam, T. M.; Rodriguez, M. A.; Cherry, B. R.; Krumhansl, J. L.; Nenoff, T. M.; Sattler, A. M. A General Synthetic Procedure for Heteropolyniobates. *Science* **2002**, *297* (5583), 996−998.
(25) Hill, C. L. In *Comprehensive Coordination Chemistry II*; McCleverty, J. A., Meyer, T. J., Eds.; Elsevier Science: New York, 2004; Vol. 4, pp 679−759.
(26) López, X.; Bo, C.; Poblet, J. M. Electronic Properties of Polyoxometalates: Electron and Proton Affinity of Mixed-Addenda Keggin and Wells−Dawson Anions. *J. Am. Chem. Soc.* **2002**, *124* (42), 12574−12582.
(27) Misra, A.; Kozma, K.; Streb, C.; Nyman, M. Beyond Charge Balance: Counter-Cations in Polyoxometalate Chemistry. *Angew. Chem., Int. Ed.* **2020**, *59* (2), 596−612.
(28) Grigoriev, V. A.; Hill, C. L.; Weinstock, I. A. Role of Cation Size in the Energy of Electron Transfer to 1:1 Polyoxometalate Ion Pairs $\{(M^+)(Xn^+VW11O40)\}(8\text{-}n)$- (M = Li, Na, K). *J. Am. Chem. Soc.* **2000**, *122* (14), 3544−3545.
(29) Grigoriev, V. A.; Cheng, D.; Hill, C. L.; Weinstock, I. A. Role of Alkali Metal Cation Size in the Energy and Rate of Electron Transfer to Solvent-Separated 1:1 $[(M^+)(\text{Acceptor})]$ ($M^+ = Li^+, Na^+, K^+$) Ion Pairs. *J. Am. Chem. Soc.* **2001**, *123* (22), 5292−5307.
(30) Wilmsmeyer, A. R.; Uzarski, J.; Barrie, P. J.; Morris, J. R. Interactions and binding energies of dimethyl methylphosphonate and dimethyl chlorophosphate with amorphous silica. *Langmuir* **2012**, *28* (30), 10962−7.

https://doi.org/10.1021/acsanm.1c00813
ACS Appl. Nano Mater. 2021, 4, 5649−5654